Indian Journal of Pure & Applied Physics
Vol. 56, June 2018, pp. 444-452

Influence of L-Lysine as dopant in ammonium tetroxalate dihydrate– spectral, optical, thermal, mechanical and dielectric properties

Eunice Jerusha[a,b], S Shahil Kirupavathy[c]* & S Shalini[a,b]

[a]Department of Physics, R M D Engineering College, Kavaripettai 601 206, India

[b]Anna University Chennai, Guindy, Chennai 600 025, India

[c]Department of Physics, Velammal Engineering College, Chennai 600 066, India

Received 9 May 2017; accepted 26 December 2017

Semi organic crystals offer a variety of molecular structures by virtue of the changes brought out in selection of dopants. In the present work mechanical, thermal, dielectric, FTIR and UV studies of single crystals of ammonium teroxalate dihydrate (ATOXAL) doped with basic amino acid L-Lysine have been studied and compared. Fourier transform infrared (FTIR) spectroscopy study confirms the incorporation of L-Lysine into ATOXAL. Optical studies on L-Lysine doped ATOXAL (L-Lys doped ATOXAL) crystals reveal that these crystals are optically better and more transparent than the pure ones having wide transmission spectra lying in the entire visible and near infrared (NIR) regions. Optical band gap has been found to be 4.281 eV and the nonlinear index of refraction is 1.829. Negative photoconductivity has been exhibited by the crystal. TG / DTG and DSC analyses reveal that thermal anomalies occurr at 111.1 °C and 231.8 °C. Low dielectric constant and dielectric loss at higher frequency observed in L-Lys doped ATOXAL is a desirable property to enhance the NLO efficiency. Also, it is observed from the dielectric studies that the ferroelectric phase has higher activation energy than the paraelectric phase. Vickers's micro hardness test reveals that dopant inclusion increased the mechanical strength of the crystals.

Keywords: Solution growth, Optical, Thermal, Dielectric, Microhardness

1 Introduction

The increasing need for cheap and easily processable materials for diverse applications has led to several studies dealing with organic, inorganic and semiorganic molecules and materials in the recent years[1,2]. Materials with the combined advantages of organic and inorganic materials called semiorganic materials are therefore more in focus. These semiorganic crystals have the collective inorganic and organic crystal properties like high damage threshold, wide transparency range, less deliquescence and high non-linear coefficient which in turn makes them suitable for device fabrication.

Certain undoped ferroelectric crystals have some disadvantages over their doped counterparts such as (i) high mobility of ferroelectric domains at room temperature, (ii) easy depolarization by electrical, mechanical and thermal means, (iii) microbial contamination with time during the growth. Therefore, organic compounds such as amino acids have been introduced in such crystals as dopants to achieve effective internal bias to stabilize the domains and to obtain the desired pyroelectric and ferroelectric properties.

The proton donor carboxyl acid (COOH) group and the proton acceptor amino (NH_2) group present in the amino acids make them interesting materials for varied applications. Moreover, amino acids are widely utilized because they contain chiral carbon atoms directing the crystallization process in the noncentrosymmetric space group, and the zwitter ionic nature favouring crystal hardness[3]. Also, it was observed from literature that there is enhancement in the material's NLO and ferroelectric properties[4,5] when amino acids are used as dopants. Hence, attempts were taken to enhance the ferroelectric behaviour of the grown ATOXAL crystal with the inclusion of amino acid dopants.

L-Lysine was selected as dopant for the present work due to its promising physical properties and various applications in biomedical areas. Also, L-lysine possesses a side chain with hydrogen atoms which offers to charge transfer to form semiorganic crystals for nonlinear optical applications[6].

The present study reports on the effect of L-Lysine as dopant on the growth and characterisation of

*Corresponding author (E-mail: shahilkirupavathy@yahoo.co.in)

ATOXAL by slow evaporation method at room temperature. The grown crystals were characterized by single crystal XRD, FTIR, UV-Vis, photoconductivity, thermal and microhardness analyses. A detailed evaluation of optical (optical band gap, extinction coefficient, refractive index, optical conductivity) and dielectric properties is also present.

2 Experimental Details

2.1 Crystal growth

Slow evaporation method was employed to grow the L-Lys doped ATOXAL crystals. Doping was achieved by adding 1, 2, 5 and 10 at. wt.% of L-Lysine with ATOXAL aqueous solution. The solution was thoroughly stirred using a magnetic stirrer for 8 h, after which it was filtered using Whatmann filter paper and transferred to clean dry petri dishes. The vessels containing the solution were covered with a perforated polythene sheet and left in a constant temperature bath which is a vibration free environment to induce crystallisation. Two weeks later crystals started nucleating and within a period of 7 days crystals had grown to a noticeable size and were ready for harvest. The as grown pure and L-Lys doped ATOXAL crystals are shown as an inset in Fig. 1.

2.2 Characterisation techniques

The grown L-Lys doped ATOXAL crystal was subjected to single crystal XRD studies using ENRAF NONIUS CAD4-F single crystal X-ray diffractometer with MoK_α (λ = 0.7107 Å) radiation. The grown crystal was ground and subjected to powder X-ray diffraction analysis with CuK_α radiation of wavelength 1.5405 Å. The Perkin Elmer spectrum two FTIR spectrometer was used to record the FTIR spectrum of L- Lys doped ATOXAL covering the region from 4000 cm^{-1} to 450 cm^{-1}. The diffuse reflectance and absorbance spectra of L-Lys doped ATOXAL crystal was recorded using the Perkin-Elmer Lambda 35 UV Winlab spectrometer. The NETZSCH STA 449F3 in N_2 atmosphere was utilised for the DSC measurement. Dielectric measurements were carried out on good quality transparent crystals from 95 ºC through the Curie point at different frequencies (50 Hz to 50 MHz) with an AC field of 1 V/cm using the HIOKI 3532-50 LCR HITESTER. The anisotropy in mechanical hardness (Vicker's microhardness number H_V) was evaluated for L-Lys doped ATOXAL crystal of 1.3 mm thickness. Hardness measurements were made with the load on $(10\bar{1})$ plane using a Shimadzu HMV-2000 fitted with a diamond pyramidal indenter and attached to an incident optical microscope.

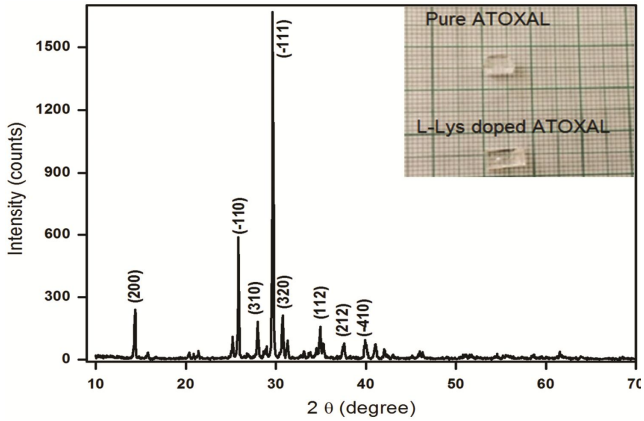

Fig. 1 – Powder XRD of L-Lys doped ATOXAL and (inset) as grown pure and L- Lys doped ATOXAL crystals.

3 Results and Discussion

3.1 Single crystal and powder X-ray diffraction

From the single crystal X-ray diffraction study, the lattice parameters and cell volume of the pure and L-Lys doped ATOXAL crystals were obtained and are given in Table 1. Single crystal X-ray diffraction data affirms that both pure[7] and L-Lys doped ATOXAL crystals belong to the triclinic system. The slight variations in the lattice parameters and cell volume of L-Lys doped ATOXAL crystal reflect the incorporation of L-Lysine molecule into the crystal lattice. The indexed powder X-ray diffraction pattern is presented in Fig. 1.

3.2 FTIR analysis

Figure 2 shows the FTIR spectrum of pure and L-Lys doped ATOXAL crystals. L-Lysine as dopant in ATOXAL produces more NH stretch vibrations which in turn results in a stronger NH absorption

Table 1 – Unit cell parameters of pure ATOXAL and L-Lys doped ATOXAL.

Unit cell parameters	Pure ATOXAL [7]	L-Lys doped ATOXAL
a (Å)	6.35	6.36
b (Å)	7.25	7.27
c (Å)	10.58	10.64
α (deg)	94.17	94.26
β (deg)	100.12	100.13
γ (deg)	97.86	97.91
V (Å^3)	472.3	478
Crystal system	Triclinic	Triclinic

peak. Also, the NH, OH and CH absorptions are stretched and overlapped into a continuum occurring at a high frequency of 3214 cm^{-1}. The few narrow bands clearly indicate the induction of amino acid L-Lysine in the lattice of ATOXAL crystal. The vibration of the OH bond is present at 2418 cm^{-1}. The asymmetric and symmetric vibrations (Table 2) of C=O in the carboxylic group are seen at 1717 cm^{-1} and 1400 cm^{-1}, respectively. Other vibrations such as the C-C and NH^{4+} are masked by the symmetric C=O vibration. Weak asymmetric NH^{3+} bonding is at 1628 cm^{-1}. Occurrence of the CH bond rocking is at 1221 cm^{-1}. The vibration and stretching of the C-C bond is seen at 1108 cm^{-1} and 808 cm^{-1}, respectively. The peak at 719 cm^{-1} represents the vibration of OH bond and the deformation vibration of O-C=O bond. Surprisingly, the bands arising from deformation vibrations of CCN groups are noticed at higher frequencies of 587 cm^{-1} and 500 cm^{-1} than that perceived in literature[8]. Thus, the FTIR spectral analysis confirms the presence of L-Lysine in the crystal lattice.

Table 2 – Vibrational assignments of L-Lys doped ATOXAL.

Wavenumbers (cm^{-1})		Assignments
L-Lys doped ATOXAL	Pure ATOXAL	
3214	3226	ν(OH) H_2O
2418		ν(OH) hydrogen bond
1717, 1701	1692	ν_{as}(C=O) COOH
1628		Weak asymmetric NH^{3+} bonding
1400	1400	ν_s(C=O), ν(C-C), NH_4^+
1277	1251	ν(C-OH)
1221		ρ(C-H)
1108		ν(C-C)
878		C-C stretching
854		O–H· · ·O out-of-plane bending
719	719	ν(OH), δ(O-C=O)
587		γ(CO), γ(CN), δ(CCN)
500	500	Deformation band

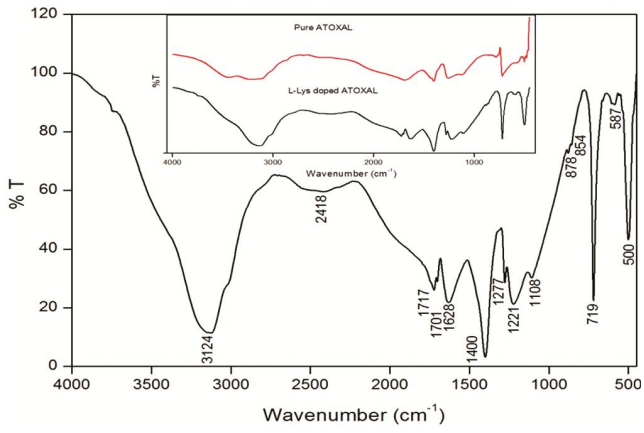

Fig. 2 – FTIR spectrum of pure and L-L Lys doped ATOXAL.

3.3 UV-Vis-NIR analysis

Ultraviolet, visible, and infrared absorption bands result from the absorption of electromagnetic radiation by specific valence electrons or bonds of low excitation energy on certain functional groups since the energy at which the absorption occurs and its intensity is determined by the chemical environment of the absorbing moiety. The absorption bands can also be correlated to the chemical structure.

3.3.1 Diffused reflectance spectroscopic studies

The transformed Kubelka-Munk spectrum for L-Lys doped ATOXAL is shown in Fig. 3. The Kubelka-Munk (K-M) function $f(R)$ or absorption coefficient α is given by:

$$f(R)=\frac{K}{S}=\frac{(1-R)^2}{2R} \quad \text{... (1)}$$

where K, S and R are the Kubleka-Munk absorption, scattering coefficients and the reflectance, respectively. The relationship between the transformed K-M function $f(R)$, the optical band gap energy E_g and the incident photon energy $h\nu$ are related by the equation:

$$(f(R)h\nu)^p = A(h\nu - E_g) \quad \text{... (2)}$$

where A is the transition probability constant and p is the power index. The extrapolation of the linear part

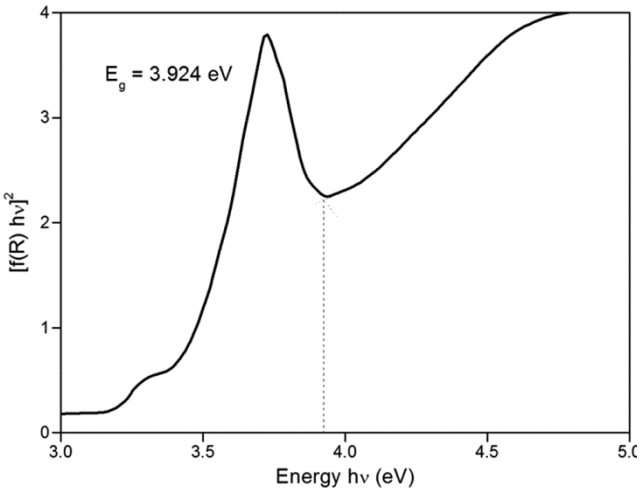

Fig. 3 – Transformed Kubelka-Munk spectrum for L- Lys doped ATOXAL.

of the $(f(R)h\nu)^2$ plot gives the optical band gap to be 3.924 eV.

3.3.2 Absorbance / transmittance studies

The transparency cut off wavelength and optical transmittance range play a vital role in determining the optical applications of the crystal. L-Lys doped ATOXAL crystal has high transmittance in the visible and NIR regions suggesting the suitability of the crystal in optoelectronics applications. There is no transmission up to 318 nm revealing that the crystal absorbs the entire UV region. Such high absorbance of UV rays observed from the spectrum suggests that the title material can be considered to be used as an effective UV filter for the prevention of melanoma or skin cancer[9-11]. The calculated value of the crystal's optical band gap energy is 3.899 eV.

The electronic states in materials can be well understood by analyzing the optical conductivity[12]. The dielectric constant is mostly considered as a complex function of the frequency of the applied field because the variation of the dielectric constant with frequency reveals that the material's polarization does not respond immediately to the applied field. Though, conductivity of a perfect dielectric material is zero, crystals possessing low dielectric loss prevents the propagation of electromagnetic energy which in turn aids conductivity. The one component or anomalous Drude model states that both the carrier relaxation time and the effective mass of the charges are functions of photon frequency ω. Contrarily, the real part of the optical conductivity σ of the crystal in the multi component model uses the following relations[13,14]:

$$\sigma = \frac{\omega}{4\pi}\mathrm{Im}(\varepsilon) = \frac{\omega}{4\pi}\times\left(\frac{c}{\omega}\right)^2 \frac{k\alpha}{\mu_r} \quad \ldots (3)$$

where μ_r is the relative permeability (≈ 1) at optical frequencies for crystalline materials. Thus, the frequency response of optical conductivity when the sample is irradiated with light is given by:

$$\sigma = \frac{\alpha n c}{4\pi} \quad \ldots (4)$$

Hence, the optical conductivity increases with an increase of photon energy. The calculated value of optical conductivity has a high magnitude of (10^{10} $\Omega^{-1}m^{-1}$). This very high photo response in the material makes it an eligible and suitable candidate for information processing and computing[15].

The absorption loss of the electromagnetic wave propagating through a material is indicated by the extinction coefficient. The dependence of extinction coefficient on the absorption coefficient is given by the expression:

$$K = \frac{\lambda\alpha}{4\pi} \quad \ldots (5)$$

The value of the absorption coefficient is calculated from the relation:

$$\alpha = \frac{1}{t}\ln\left(\frac{1}{T}\right) \quad \ldots (6)$$

For small photon energy $h\nu$ and allowed optical transition, the general equation for the band gap energy estimation is:

$$(\alpha h\nu)^2 = A\left(h\nu - E^t\right) \quad \ldots (7)$$

where A is the disorder parameter and E^t is the transition energy. The bandgap was found to be 3.912 eV from the plot of $(\alpha h\nu)^2$ versus $h\nu$ portrayed in Fig. 4. The relation between reflectance R and absorption coefficient is given by:

$$R = \frac{1 \pm \sqrt{1 - e^{-\alpha t} + e^{\alpha t}}}{1 + e^{\alpha t}} \quad \ldots (8)$$

The refractive index n can be calculated from reflectance data[16]. The low reflectance and extinction values observed imply high transmittance of the grown crystal and its suitability for device fabrication respectively. The refractive index of L-Lys doped ATOXAL thus obtained at the cutoff wavelength is 1.785.

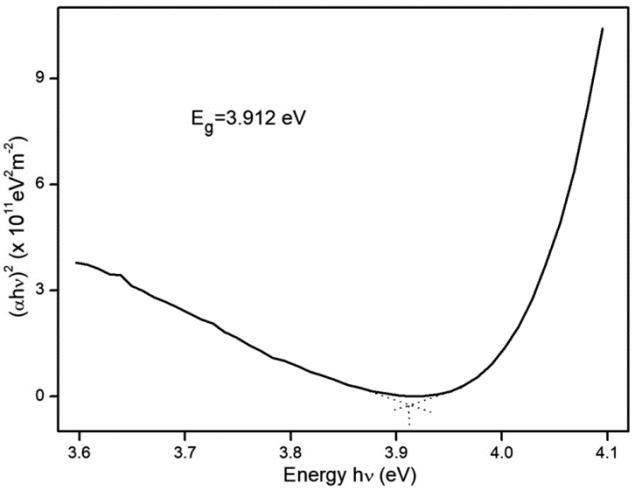

Fig. 4 – Determination of optical bandgap E_g in L- Lys doped ATOXAL.

The optical properties of the material are computed from the complex dielectric constant ε as described by Gupta *et al.*[17]. The calculated values of the real ε_r and imaginary ε_i dielectric constants and electric susceptibility χ_c are 3.188, 0.132×10^{-5} and 0.254, respectively, at the cutoff wavelength.

3.4 Photoconductivity

The field dependent dark and photo currents of L-Lys doped ATOXAL crystal is shown in Fig. 5. It is observed that negative photoconductivity is exhibited when the dark current is found to be higher than the photocurrent. This behaviour may be attributed due to the reduction in charge carrier concentration or lifetime in the presence of illumination. Lifetime reduction with intense radiation[18], is due to trapping of charge carriers and an increase in carrier velocity v in accordance with the relation:

$$\tau = (vsN)^{-1} \quad \ldots (9)$$

where s is the capture cross section of the recombination centers and N is the carrier concentration. Stockmann model consisting of a two level (upper and lower energy levels) scheme explains the negative photoconductivity[19] exhibited by the material. According to this model, the upper energy level is positioned closer to the conduction band and the lower energy level is situated in the vicinity of the valence band. When the sample is exposed to light, the high capture cross section of the lower energy level for electrons from the conduction band and holes from the valence band results in the immediate recombination of electrons and holes. Hence, there is a decrease in the number of mobile charge carriers, leading to negative photoconductivity.

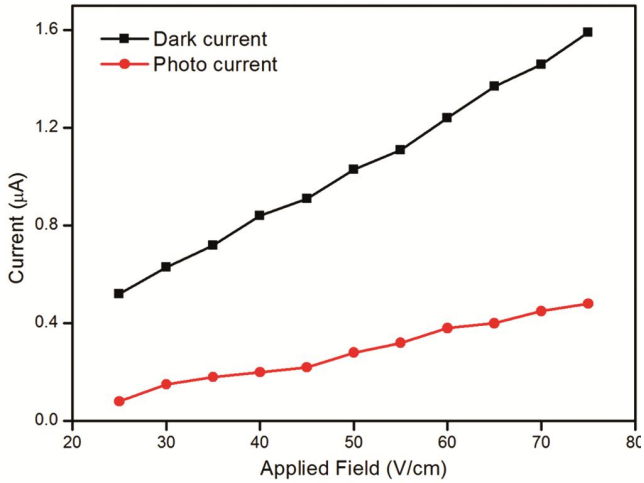

Fig. 5 – Photo and dark currents in L- Lys doped ATOXAL.

3.5 Thermal analysis

The thermal stability of any material is crucial for any potential application. In order to know the thermal stability of the material, thermogravimetric analysis (TGA) as well as differential thermogravimetric analysis (DTG) was carried out on L- Lys doped ATOXAL in N_2 ambience. The TG/DTG thermogram is shown in Fig. 6 and the DSC curve is seen in the inset of Fig. 6. The peak observed in the DSC curve at 111.1 ºC is a thermal anomaly indicating the phase transition occurring in the sample and the second peak at 231.8 ºC is another anomaly which may be due to the loss of the water molecules and the subsequent decomposition of the title material. These anomalies have been duly supported by the inflections in the TG / DTG analysis.

3.6 Dielectric analysis

Dielectric property changes which are observed in L-Lys doped ATOXAL compared to the parent material ATOXAL may be ascribed to the local strain caused by the high dipole moment of the L-Lysine molecules[20].

The dielectric properties of L-Lys doped ATOXAL were explored by studying the frequency dependence of the dielectric constant and dielectric loss. Both dielectric constant and dielectric loss decrease gradually with increasing frequency. The decrease of ε´ in a polar material with frequency can be attributed to the total contribution of deformational (electronic and ionic) and relaxation (orientational and

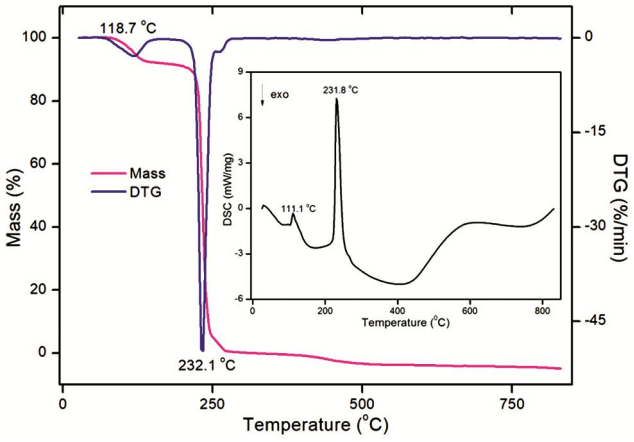

Fig. 6 – TG / DTG analysis of L-Lys doped ATOXAL; (inset) DSC curve of L-Lys doped ATOXAL.

interfacial) polarizations. When the frequency is increased, the orientational polarization decreases since it takes more time than electronic and ionic polarization. The constant value of dielectric constant ε′ at higher frequency corresponds to interfacial polarization.

The decrease in the imaginary part of the dielectric constant ε″ with increasing frequency is owing to the migration and vibrations of ions. According to the theory of hopping of charge carriers over a potential barrier between charged defects[21-23] ε″ can be expressed by the following relation:

$$\varepsilon'' = A\omega^{m} \quad \text{... (10)}$$

$$\text{with } m = -\frac{4k_B T}{W_m} \quad \text{... (11)}$$

where A is a constant, W_m is the maximum barrier height and m is the temperature dependent frequency power parameter. The value of m for various dopant concentrations is obtained from the slope of the variation of log ε″ with log ω plotted in Fig. 7. The maximum barrier height W_m calculated for these varied concentrations are presented in the same plot.

The absence of any peak in the dielectric loss of the material suggests the behaviour of L-Lys doped ATOXAL to be that of low-frequency dispersion (LFD) or the quasi-dc process[24-28] (QDC). This could be a carrier-dominated system exhibiting QDC responses. In QDC process no loss peak is observed.

Facilitation of dipole orientation increases the value of orientational polarization, which in turn increases the dielectric constant ε′ with temperature. Also, the degree of crystallinity increases[29-31] ε′. Determination of T_m the ferroelectric transition temperature, T_C the Curie temperature and T_{CW} the Curie-Weiss temperature is done from the plot of $\frac{1}{\varepsilon'}$ against temperature. The variation of these temperatures with dopant concentrations is presented in Fig. 8.

The temperature dependent variation of the electrical susceptibility χ shown in Fig. 9 obeys the Curie-Weiss law:

$$\chi = \frac{A}{T - T_C} \quad \text{... (12)}$$

Systems exhibiting QDC process have their susceptibility increasing rapidly towards low

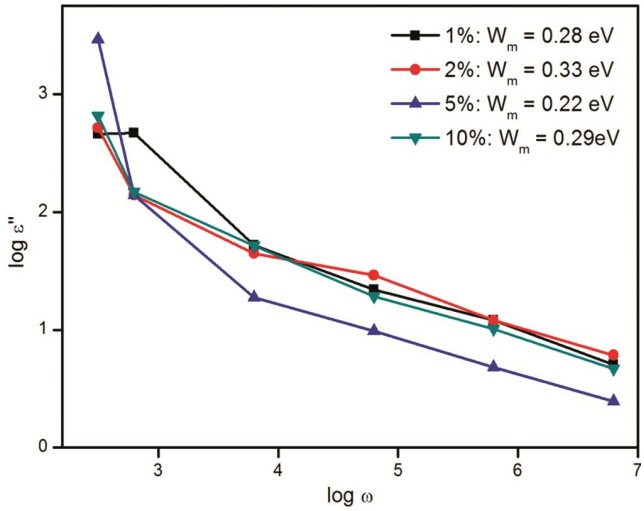

Fig. 7 – Plot of log ε″ with log ω for L-Lys doped ATOXAL.

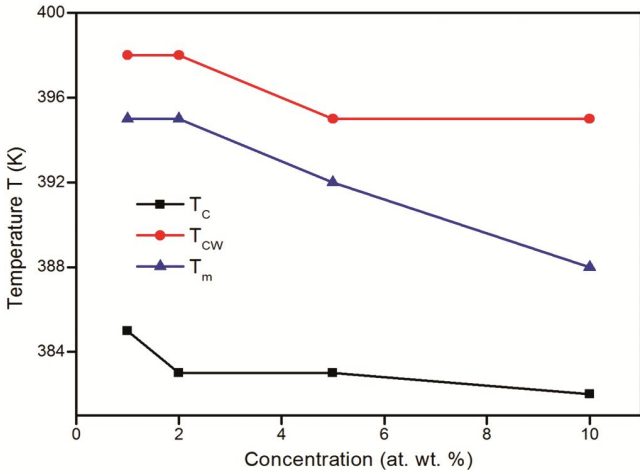

Fig. 8 – Variation of T_{CW}, T_m and T_C for various concentrations of L-Lysine as dopant in ATOXAL.

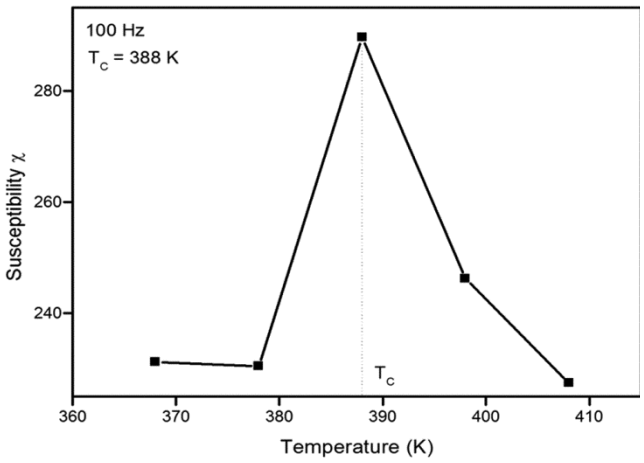

Fig. 9 – Variation of susceptibility χ with temperature T in L-Lys doped ATOXAL.

frequencies without any sign of saturation. Also, they follow a parallel trend in a log–log representation and obey a power law of the type:

$$\chi = \omega^{n-1}; 0 < n < 1 \quad \text{... (13)}$$

where χ is the electric susceptibility of the material which is related to real dielectric constant as :

$$\chi = \varepsilon' - 1 \quad \text{... (14)}$$

For the title material, the values of n at various temperatures are obtained from the plot of logχ versus log ω shown in Fig. 10. It is observed that the value of n is the least at the phase transition temperature. The universal fractional power law is obeyed by a variety of solid materials, including low loss dielectrics, dipolar materials, hopping electronic systems, ionic conductors, semiconductors, *p–n* junctions, interfacial phenomena, and mechanical relaxation[28]. Jonscher's power law is obeyed for the behaviour of conductivity with frequency[32,33] as:

$$\sigma(\omega) = \sigma_0 + A\omega^p \quad \text{... (15)}$$

where σ_0 is the low frequency independent DC conductivity and $\omega = 2\pi f$ is the angular frequency, p is the power law exponent which lies[34] between 0 and 1 and is calculated from the plot of ln σ versus ln ω at varied temperatures. The trend of the curve indicates that the conduction mechanism is by the hopping of protons through hydrogen bonds or of mobile charge carriers (ions) over the barrier between two sites. The variation of exponent p with temperature for various concentrations of the dopant is shown in Fig. 11. The change of p with the temperature corresponds to a thermally activated process.

The behaviour of p governs the charge transport mechanism[35-37] of conductivity σ. There are two types of charge transport mechanisms; the quantum mechanical tunnelling[38,39] (QMT) and the classical hopping over a barrier[40] (HOB). For the first mechanism, the frequency exponent p is independent of temperature but dependent on frequency. However, from Fig. 11 we see that the curve trend is contradictory to the above model and it is evident that the frequency exponent decreases with an increase of temperature. Alternatively, for the HOB model the value of p must equal unity. Therefore, it is clear that at higher dopant concentrations, p would approach unity and the HOB model would be deemed fit to explain the mechanism of conduction in L- Lys doped ATOXAL.

The plot of ln σ against $\frac{1000}{T}$ seen in Fig. 12, shows that the higher frequency response is totally temperature independent and the lower frequency

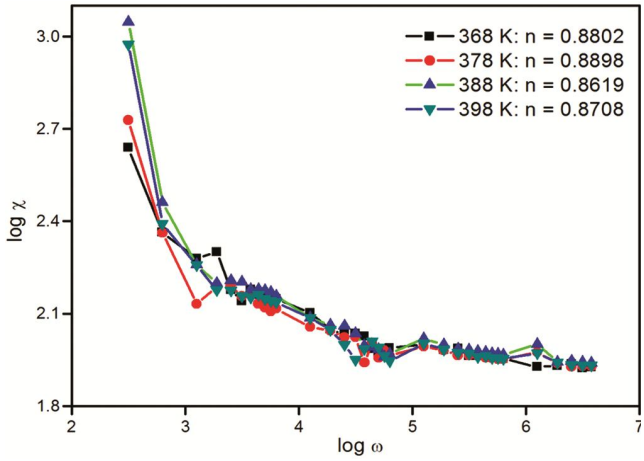

Fig. 10 – Variation of log χ with log ω in L-Lys doped ATOXAL.

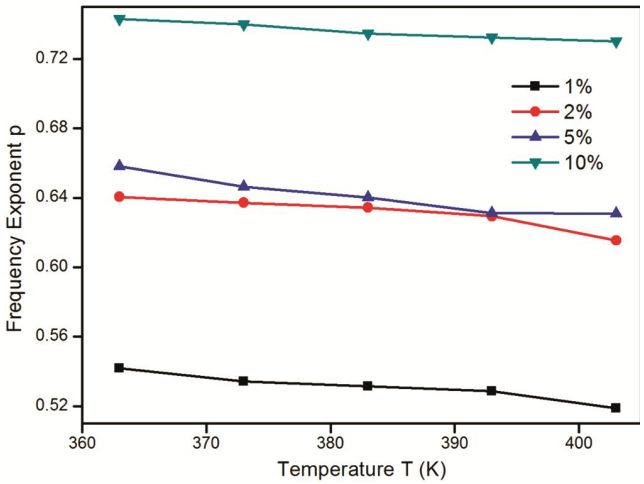

Fig. 11 – Plot of ln σ against ln ω in L-Lys doped ATOXAL.

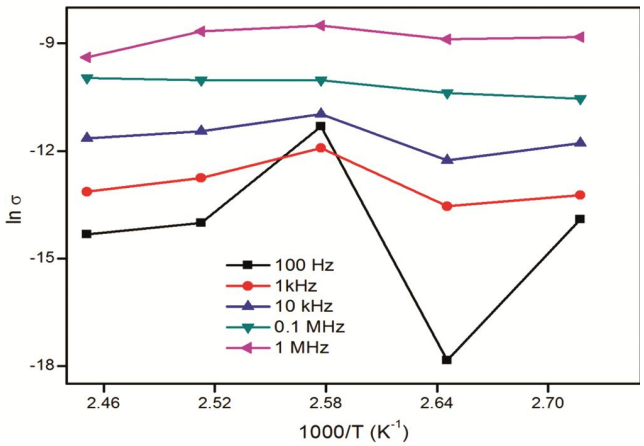

Fig. 12 – Variation of frequency exponent p with temperature T for various concentrations of L-Lysine in ATOXAL.

response revealed two temperature regimes. One, varying linearly with temperature (strongly dependent) and the other, nearly independent of temperature (weakly dependent). Also, at the phase transition temperature two different slopes are observed on either side of the peak suggesting different activation energies for the ferroelectric and paraelectric phases. The ferroelectric phase has higher activation energy than the paraelectric phase as depicted in Fig. 13. The first region observed at lower temperatures is due to impurities and may be attributed to the ordered state of ferroelectric phase and the second region that occurred at higher temperature is due to polaron hopping and may be attributed to disordered paraelectric state. It is also observed that, the rate of decrease of resistivity is slow up to the transition temperature and there after it decreases rapidly. The conduction is due to large effective mass and low mobility of current carriers. The lowering of the activation energy is attributed to the effect of spin ordering[41].

3.7 Microhardness study

The structure and composition[42] (i.e., presence of an additional phase or phase transition and inherent lattice imperfections) of the crystals are inviolably related to the mechanical hardness. Microhardness testing is one of the best methods of understanding the mechanical properties of materials such as fracture behaviour, yield strength, brittleness index and temperature of cracking[43-45].

Loads ranging from 1 g to 200 g were used for indentations with the time of indentation constant at 10 s. The diagonal length of the indentation impression for various loads was measured using the micrometer eyepiece at a higher magnification.

The Vicker's microhardness value[46] H_V was determined using

$$H_V = 1.8544\frac{P}{d^2} \quad \text{kgmm}^{-2} \qquad \text{... (16)}$$

where H_V is the Vicker's microhardness number, P is the applied load and d is the average diagonal length of the indentation mark. Hardness is low at relatively low loads and it increases with higher loads until the development of cracks at 10 g around the indent. This is due to the release of internal stress generated locally by the indentation. Doped crystals have relatively higher hardness than undoped ones. Increase in bond energy with doping is assumed to be the cause for higher hardness values[47].

The variation of H_V with load P is seen in Fig. 14 and the inset shows the plot obtained between log P against log d for the L-Lys doped ATOXAL crystal. A straight line is derived from Meyer's law:

$$P = k_1 d^n \qquad \text{... (17)}$$

where k_1 is the standard hardness value and n is the Meyer's index number or work hardening coefficient. The slope of the curve in the inset of Fig. 14 gives n as 3.153 and satisfies the prediction of Onitsch[48]. Other load dependent parameters such as the standard hardness values k_1 and k_2, fracture toughness K_C, brittleness index B_i and yield strength σ_y are calculated and given in Table 3.

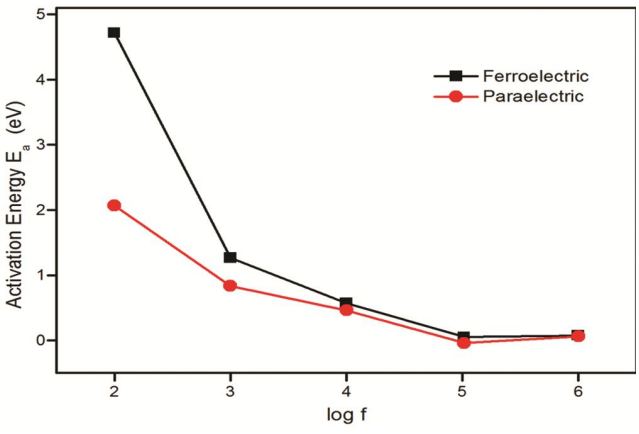

Fig. 13 – Variation of the ferroelectric and paraelectric activation energies in L-Lys doped ATOXAL.

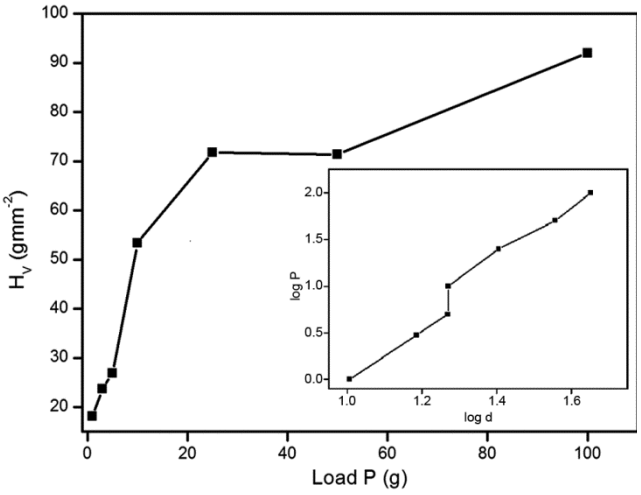

Fig. 14 – Variation of H_V with P in L-Lys doped ATOXAL (inset) Plot of log P against log d in L-Lys doped ATOXAL.

Table 3 – Microhardness parameters for L-Lys doped ATOXAL.

Sample	H_V kg/mm^2	n	k_1 × 10^5 kg/m	k_2 × 10^4 kg/m	W × 10^{-3} kg	c_{11} × 10^{14} Pa	x μm	σ_y MPa
Pure ATOXAL	39.98	2.917	4.017	3.844	16.07	635.83	-0.0105	2.168
L-Lys doped ATOXAL	53.372	3.153	2.048	2.345	10.239	1068.63	-0.0023	2.879

4 Conclusions

L-Lys doped ATOXAL single crystals were grown by the slow evaporation solution growth method. Lattice parameters were found from the single crystal X-ray diffraction data. FTIR spectrum confirmed the qualitative presence of the amino acid L-Lysine. A marginal decrease in the optical band gap from 3.963 eV to 3.912 eV is observed on doping with an increase in optical conductivity. Negative photoconductivity is observed as that of the parent material with a slight increase in the photo and dark currents. Thermal studies reveal a 10 ºC rise in the phase transition temperature. Dielectric studies show a similar shift in the Curie temperature. Dielectric constant of L-Lys doped ATOXAL crystal was found to be lower than the pure ATOXAL crystal. Due to doping, the hardness of the crystal was decreased.

References

1 Lines M E & Glass A M, *Principles and applications of ferroelectrics and related materials*, (Oxford university press), 1977.
2 Scott J F, *Science*, 315 (2007) 954.
3 Bhat M N & Dharmaprakash S M, *J Cryst Growth*, 236 (2002) 376.
4 Dhumane N R, Hussaini S S, Dongre V G, Karmuse P P & Shirsat M D, *J Cryst Res Technol*, 44 (2009) 269.
5 Brown P T, Ross G W, Eason R W & Pogosyan A R, *Opt Commun*, 163 (1999) 310.
6 Ramesh B R, Vijayan N, Gopalakrishnan R & Ramasamy P, *Cryst Res Tech*, 41 (2006) 405.
7 Eunice J, Infant Shyam K R, Shahil K S & Gopalakrishnan R, *Optik*, 127 (2016) 3896.
8 Baran J, Drozd M, Pietraszko A, Trzebiatowska M & Ratajczak H, *Pol J Chem*, 77 (2003) 1561.
9 Pleasance E D, Cheetham R K & Stephens P J, *Nature*, 463 (2009) 191.
10 Gordon L G, Scuffham P A, Vander P J C, Mc Bride P, Williams G M & Green A C, *J Invest Dermatol*, 129 (2009) 2766.
11 Fackelman K, Science News, Melanoma Madness: *The scientific flap over sunscreens and skin cancer*, 1998.
12 Arumanayagam T & Murugakoothan P, *J Min Mater Character Eng*, 10 (2011) 1225.
13 Lucarelli A, Lupi S, Calvani P & Maselli P, *Phys Rev B*, 65 (2002) 054511.
14 Ugwu E I, Olayinka A S & Olabode F I, *J Eng Appl Sci*, 4 (2009) 126.
15 Santhakumari R & Ramamurthi K, *Spectrochim Acta A*, 78 (2011) 653.
16 Hanumantharao R, Kalainathan S & Bhagavanarayana G, *Spectrochim Acta A*, 91 (2012) 345.
17 Gupta V & Mansingh A, *J Appl Phys*, 80 (1996) 1063.
18 Joshi V N, *Photoconductivity*, (Marcel Dekker: New York), 1990.
19 Bube R H, *Photoconductivity of solids*, (Wiley: New York), 1981.
20 Brabec V, Walz D & Milazzo G, *Experimental techniques in bioelectrochemistry*, Birkhāuser Verlag Basel, (Springer: Basel AG), 1996.
21 Gibson H W, Weagley R J, Prest J W M, Mosher R & Kaplan S, *J Phys Colloid Chem*, 6 (1983) 123.
22 Mott N F & Davis E A, *Electronic processes in non-crystalline materials*, (Clarendon Press: Oxford), 1979.
23 Giuntini J C & Zancheha J V, *J Non-Cryst Solids*, 34 (1979) 57.
24 Want B & Rubiya S, *J Mater Sci*, 49 (2014) 4891.
25 Jonscher A K, *Colloid Polym Sci*, 253 (1975) 231.
26 Dissado L A & Hill R M, *Proc Roy Soc London*, 390 (1983) 131.
27 Dissado L A & Hill R M, *J Chem Soc Faraday Trans*, 80 (1984) 291.
28 Jonscher A K, *IEEE Trans Electr Insul*, 27 (1992) 407.
29 Abdel-Malak T G, Kassem M E, Aly N S & Kalil S M, *Acta Phys Pol A*, 81 (1992) 675.
30 Cao W & Gerhardt R, *Solid State Ion*, 42 (1990) 213.
31 Singh R, Tandon R P, Panwar V S & Chandra S, *J Appl Phys*, 69 (1991) 2504.
32 Jonscher A K, *Nature*, 267 (1977) 673.
33 Jonscher A K, *J Mater Sci*, 16 (1981) 2037.
34 Ingram M D, *Phys Chem Glasses*, 28 (1987) 215.
35 Hazara S & Ghosh A, *Phil Mag*, 74 (1996) 235.
36 El-Nahass M M, Zeyada H M, El-Samanoudy M M & El-Menyawy E M, *J Phys Condens Matter*, 18 (2006) 5163.
37 Yakuphanoglu F, Aydogdu Y, Schatzschneider U & Rentschler E, *Solid State Commun*, 128 (2003) 63.
38 Austin G & Mott N F, *Adv Phys*, 18 (1969) 41.
39 Pollak M, *Phil Mag*, 23 (1971) 519.
40 Pollak M & Pike G E, *Phys Rev Lett*, 28 (1972) 1449.
41 Lokare S A, *Int J Chem Phys Sci*, 4 (2015) 154.
42 Krishnan S, Justin R C, Robert R, Ramanand A & Das J, *Solid State Electronics*, 52 (2008) 1157.
43 Srinivasan P, Kangasekaran T, Gopalakrishnan R, Bhagavanarayana G & Ramasamy P, *Cryst Growth Design*, 6 (2006) 1663.
44 Dawn R & Fuller E R, *J Mater Sci*, 9 (1975) 2016.
45 Westbrook J H, *Report 58-RL-2033 of the G E Research Laboratory*, USA, 1958.
46 Mott W, *Micro-indentation hardness testing*, (Butterworths Scientific Publications: London), 1956.
47 Mohan K R, Muralidharan R, Rajan B D, Rajendran K V, Jayavel R, Jayaraman D & Ramasamy P, *J Cryst Growth*, 229 (2001) 568.
48 Onitsch M, *Microskope*, 95 (1950) 12.